JCI insight

VentX expression in tumor associated macrophages promotes phagocytosis and immunity against pancreatic cancers

Yi Le, … , Thomas Clancy, Zhenglun Zhu

JCI Insight. 2020. https://doi.org/10.1172/jci.insight.137088.

Research In-Press Preview **Immunology**

Pancreatic ductal adenocarcinoma (PDA) is a lethal malignancy that has no effective treatment. The tumor microenvironment (TME) of PDA employs a multitude of immune derangement strategies to protect PDA from immune elimination. Tumor associated macrophages (TAMs) have been implicated in pathogenesis of immune suppression of PDA-TME, however, its underlying mechanisms remained largely unknown. Using primary patient samples, our studies showed that in comparison with macrophages isolated from normal pancreatic tissues, the phagocytosis activity of PDA-TAM is significantly reduced. We found that the expression of homeobox protein VentX, a master regulator of macrophage plasticity, is significantly decreased in the PDA-TAMs. We demonstrated that VentX is required for phagocytosis and that restoration of VentX expression in PDA-TAMs promotes phagocytosis through regulating the signaling cascades involved in the process. Using an ex-vivo culture model of primary human PDA, we showed that VentX-modulated-TAMs transformed PDA-TME from a pro-tumor milieu to an anti-tumor microenvironment by rectifying differentiation, proliferation and activation of PDA-infiltrating immune cells. Using NSG-PDX models of primary human PDAs, we showed that VentX-modulated-TAMs exert strong inhibition on PDA tumorigenesis in vivo. Taken together, our data revealed a central mechanism underlying immune evasion of PDA and a potential novel venue to improve PDA prognosis.

VentX expression in tumor associated macrophages promotes phagocytosis and immunity against pancreatic cancers

Yi Le[1], Hong Gao[2], William Richards[3], Lei Zhao[4], Ronald Bleday[3], Thomas Clancy[3] and Zhenglun Zhu[1]

[1]Department of Medicine, [3]Department of Surgery and [4]Department of Pathology, Brigham and Women's Hospital, [2]Department of Medicine, Tufts Medical Center, Boston, Massachusetts

*Running title: *VentX promotes phagocytosis and immunity*

To whom correspondence should be addressed: Zhenglun Zhu, Department of Medicine, Brigham and Women's Hospital, Boston, MA 02115, Tel.: 617-732-5467; Fax: 617-730-5807; Email: zzhu@partners.org

Abstract:

Pancreatic ductal adenocarcinoma (PDA) is a lethal malignancy that has no effective treatment. The tumor microenvironment (TME) of PDA employs a multitude of immune derangement strategies to protect PDA from immune elimination. Tumor associated macrophages (TAMs) have been implicated in pathogenesis of immune suppression of PDA-TME, however, its underlying mechanisms remained largely unknown. Using primary patient samples, our studies showed that in comparison with macrophages isolated from normal pancreatic tissues, the phagocytosis activity of PDA-TAM is significantly reduced. We found that the expression of homeobox protein VentX, a master regulator of macrophage plasticity, is significantly decreased in the PDA-TAMs. We demonstrated that VentX is required for phagocytosis and that restoration of VentX expression in PDA-TAMs promotes phagocytosis through regulating the signaling cascades involved in the process. Using an *ex-vivo* culture model of primary human PDA, we showed that VentX-modulated-TAMs transformed PDA-TME from a pro-tumor milieu to an anti-tumor microenvironment by rectifying differentiation, proliferation and activation of PDA-infiltrating immune cells. Using NSG-PDX models of primary human PDAs, we showed that VentX-modulated-TAMs exert strong inhibition on PDA tumorigenesis in vivo. Taken together, our data revealed a central mechanism underlying immune evasion of PDA and a potential novel venue to improve PDA prognosis.

Introduction

Pancreatic ductal adenocarcinoma (PDA) is one of the most lethal malignancy with median survival of less than one year and overall 5-year survival less than 5% (1, 2). Despite exciting progress, current immune therapeutic modalities have shown limited efficacy against PDA (3). Without effective therapeutic option in sight, currently, the PDA mortality closely parallels to its raising incidence and is expected to be the 2nd leading cause of cancer related death in 2030 (4, 5).

Over the past decades, extensive investigations indicated the role of PDA tumor microenvironment (TME) in rendering PDA resistance to current treatment modalities (6). Different from immune responsive cancer types, such as the non-small cell lung cancer (NSCLC), renal cell carcinoma (RCC) and melanoma, the PDA-TME demonstrated unique features with a multitude of immune derangement to protect PDA from immune elimination (7, 8). In the PDA-TME, there is a paucity of the cytotoxic CD8 T cells but increased prevalence of immune suppressive Treg Cells (9, 10). Moreover, the PDA-TME contains significant numbers of tumor associated microphages (TAMs), which display a pro-tumor M2-like phenotype (11, 12). In comparison with melanoma, PDA-TAMs expresses higher levels of immune check point inhibitors, Vista, but lower level of PD-L1 (13). Collectively, these molecular and cellular composition of the PDA-TME constitute an immune privileged environment to protect PDA as a "cold tumor" (3). Despite wild speculation, the rudimental cause of PDA immune evasion remained largely unknown and methods to reverse the immune suppression at PDA-TME remained far-reach.

TAM is a major component of PDA-TME. Using clinical samples obtained from primary PDA patients, we observed that phagocytosis, the essential macrophage function in antigen presentation and immune surveillance, is significant impaired in PDA-TAMs. To define the mechanism underling the TAM inertia, we found that the expression of homeobox protein VentX, the master regulator of macrophage plasticity (14), is drastically reduced in TAMs of all tested cases of PDA. We showed that restoration of VentX expression in PDA-TAMs recovers its phagocytosis function. Mechanistically, we showed that VentX promotes the expression of cell surface receptor, such as TLRs and controls intracellular signaling cascades involved in phagocytosis. Consistent with its

role in polarizing TAMs from the pro-tumor M2-like phenotype to the anti-tumor M1-like phenotype, we demonstrated that VentX-modulated-TAMs transform PDA-TME from immune suppression to immune activation through alternating the molecular and cellular compositions at the PDA-TME. Using a pre-clinical model of primary human PDA, we showed that VentX-modulated-TAMs exerts strong inhibition of PDA tumorigenesis in vivo. Taken together, our studies suggested a key regulatory role VentX in governing the fundamental function of macrophages and a central function of VentX-TAMs in modulating immunity at PDA-TME. Our study suggested a potential novel venue of immunotherapy of PDA, functioning in part, by promoting phagocytosis and rectifying immune derangement at PDA-TME.

Results

Characterization of PDA-TME, VentX expression is decreased in PDA-TAMs

To better understand the mechanism underlying immune suppression at the PDA-TME, we characterized the composition and function of immune cells at PDA-TME. Tumor associated macrophages and T cells were isolated from fresh PDA and adjacent normal tissues, which were verified by board certified pathologist. Consistent with prior immunohistochemistry findings (15), in comparison with adjacent normal tissues, the PDA-TME contains significantly increased numbers of macrophages, which predominately display a characteristic M2-like phenotype (Figure 1). Consistent with its immune suppressive function in PDA-TME, the PDA-TAMs express increased levels of immune suppressive cytokines, such as the IL-4, IL-10, IL13 and TGF-β but decreased levels of pro-inflammatory cytokines, IL-1b, IL-8, IL-12B and TNF-α, (Figure 2A). In addition, the PDA-TAMs express increased levels of immune check point inhibitors, such as the PD-L1 and Vista (Figure 2B). Similar to the TME of colorectal cancer (CRC), the prominent presence of M2-like TAMs in PDA-TME is accompanied by a significantly increased number of immune suppressive Treg cells. In contrast, there were very limited numbers of cytotoxic effector CD8 T cells in PDA-TME (Supplemental Figure 2).

As the key executor of both innate and adaptive immunity, TAMs have been implicated in immune suppression at TME (16). On the premise of our recent findings of

the homeobox protein VentX as the master regulator of macrophage plasticity and its implications in pathogenesis of immune suppression at TME (14, 17, 18), we further explored the potential involvement of VentX in immunopathogenesis of PDA. We found that, similar to its involvement of colorectal cancer (CRC) (18), the expression of VentX is significantly decreased in TAMs of all tested cases of PDA (Figure 2C and 2D).

Restoration of VentX expression in PDA-TAMs promotes phagocytosis

Phagocytosis constitutes the essential effector function of macrophages (19). While implicated in antitumor immunity, the role and mechanisms of phagocytosis in pathogenesis of PDA remained poorly defined. Using primary clinical samples, we sought to determine whether phagocytosis function of TAMs is compromised in PDA-TME. To achieve our goal, PDA-TAMs and control macrophages were isolated from PDA and adjacent normal pancreatic tissues. Using an *ex-vivo* phagocytosis assay of CFSE-labeled pancreatic cancer cells, we found that the phagocytic activities of PDA-TAMs is significantly impaired in comparison to the macrophages isolated from adjacent normal pancreatic tissues (Figure 3A). Consistent with its functional plasticity, previous studies suggested that phagocytosis is regulated by M1 and M2 signals (20). As such, our findings that VentX, the master controller of macrophage plasticity, is significantly down-regulated in PDA-TAMs prompted us to explore whether VentX regulates phagocytic function of PDA-TAMs. To attend our goal, we transfected the primary PDA-TAMs with plasmid encoding GFP-VentX or control GFP and found that ectopic expression of VentX led to 2.5-3 folds increase of PDA-TAM phagocytosis (Figure 3B). The effects of VentX on PDA-TAM phagocytosis can be readily visualized with phase contrast and fluorescent microscopy examination of the co-culture of PDA-TAMs and CFSE-yellow-labeled tumor cells (Figure 3B and 3C). To rule out the possibility that VentX promotion of phagocytosis is cell type specific, we tested the effects of VentX expression on PDA-TAM phagocytosis of leukemia cells and found that VentX promotes phagocytosis indiscriminately (Supplemental Figure 3). In addition to its effects in promoting phagocytosis, when a time-course observation of phagocytosis was performed, we found that after the CFSE-labeled cells were engulfed during the first 24 hours, the CFSE dyes became diffusely distributed throughout the cell in 24 to 48 hours (Figure

3C). There were no formation of foamy cell and accumulation of vacuole of uncleared phagocytic material as observed in M2 macrophages (21). Indeed, consistent with our prior findings in CRC-TAMs (18), we found that ectopic expression of VentX in PDA-TAMs promotes the polarization of PDA-TAMs from the M2-like phenotype to M1-like phenotype (Supplemental Figure 4). We showed that VentX inhibits the cell surface expression of M2 marker CD163 but promote the expression of M1 marker CD80 (Supplemental Figure 4A); VentX also promotes the expression and secretion of pro-inflammatory cytokines, TNF-α, IL-1β and IL-12 but inhibits the expression of immune suppressive cytokines, TGF-β, IL-4 and IL-10 (Supplemental Figure 4C and 4D). Moreover, we found that VentX expression in PDA-TAMs inhibits the expression of immune check point blockade proteins PD-L1 and Vista and promotes the expression and secretion of effector molecules, such as Nitrate (Supplemental Figure 4B and 4E).

To explore the mechanisms underlying VentX promotion of phagocytosis, we performed a targeted screen of cell surface receptors and signaling pathways implicated in phagocytosis. We found that VentX promotes the expression of TLR2 and TLR9 and downstream signaling molecules MyD88 and MAP kinase p38 in PDA-TAMs (Figure 4A). In comparison, ectopic expression of VentX in PDA-TAMs exerts little effect on the expression of SIRPα , the cellular receptor for CD47, the "do not eat me" signal implicated in cancer immune evasion (22)(Figure 4B). Instead, we found that VentX expression inhibits the phosphorylation of SHP-1 and SHP-2, the SIRPα downstream signaling molecules implicated in inhibition of phagocytosis. Moreover, we found that VentX expression promotes the phosphorylation of FAK kinase implicated in promoting phagocytosis (Figure 4C). Consistent with the essential requirement of VentX in phagocytic function of PDA-TAMs, we found that when the PDA-TAMs were treated with morpholino-oligo against VentX, the stimulation effects of LPS was abolished (Figure 4D). Our findings suggested an essential role of VentX in regulating the balance of signaling cascades to promote phagocytosis.

VentX-TAMs transforms PDA-TME and promotes immunity against PDA.

A multitude of immune derangement of the PDA-TME has been implicated in PDA evasion of current immune therapeutic modalities. Macrophages are key executor of both innate and adaptive immunity. Our findings that VentX promotes PDA-TAM phagocytosis and polarizes PDA-TAMs from the M2 like phenotypes to the M1 like phenotypes prompted us to examine the effects of VentX-modulated-PDA-TAMs on immune state of PDA-TME. To attend our goal, fresh isolated PDA-TAMs were transfected with plasmid encoding GFP-VentX (VentX-TAMs) or control GFP (Control-TAMs). The VentX-TAMs or the control-TAMs were then co-cultured with en block autologous PDA-tissues. The composition of immune cells at the PDA-TME were analyzed five days later. We found that in compassion with the control GFP-TAMs, co-culturing VentX-TAMs led to about 3 folds increases of the M1-like TAMs and more than 5 folds decreases of the M2-like TAMs in PDA-TME (Figure 5A). In parallel to the switch of the M1 vs M2 ratio, there was about 4 folds reduction in the number of inhibitory Treg cells and more than 4 folds increase of the cytotoxic CD8 T cells in PDA-TME (Figure 5 B and C). Besides FACS analysis, we also examined immune cell composition of the PDA-TME by immunohistochemistry. Consistent with the FACS findings, immunohistochemistry analysis of thin section of PDA before and after the co-culturing with VentX-TAMs showed dramatic reduction of the M2-like TAMs and marked increases in the number of cytotoxic CD8 T cells (Figure 5D). To explore the mechanisms underlying the alternation of cellular composition at the PDA-TME, we co-cultured CD8 T cells with autologous PDA-TAMs transfected with GFP-VentX or control GFP and found that VentX abolished the inhibitory effects of PDA-TAMs on CD8 proliferation and activation (Supplemental Figure 5). Together with the effects of VentX on PDA-TAM phenotypes and the expression of immune check point inhibitors (Supplemental Figure 4), our data suggested that VentX-TAMs transform the immune status of PDA-TME by rectifying a multitude of molecular and cellular derangement at PDA-TME. As the M1/M2 ration and the CD8/Treg ratio have been implicated in PDA prognosis (11), we sought to explore the therapeutic potential of VentX-TAM on PDA. As VentX does not have a murine homologue (23), to attend our goal, we transplant a small piece of primary human PDA tissue subcutaneously at the dorsal lateral side of NSG mice to generate the NSG-PDX model of primary human PDA. Seven days post-

transplantation, the NSG-PDA mice were tail vein injected with VentX-TAMs or control GFP-TAMs. Consistent with the tumor chemokine-traction of macrophages (24, 25), we found that the injected TAMs accumulated in lymph nodes on the side of transplanted tumors (Figure 6A). In addition, we also observed the homing of the injected VentX-TAMs to the implanted PDA (Supplemental Figure 6B). The effects of VentX-TAMs on the growth of PDA in vivo was observed for up to 6 weeks. As shown in Figure 6B, in comparison with the control GFP-TAMs treated mice, VentX-TAMs exerts strong inhibition on the growth of PDA in the NSG-PDX model of primary human PDA.

Discussion

Phagocytosis underlies the fundamental function of macrophages for antigen presentation and immunosurveillance. However, the role of phagocytosis in tumorigenesis remains an area of active debate (26). Previous studies suggested that inhibition of phagocytosis may plays an important role in tumor evasion of immune surveillance. It was shown that the expression of CD47, the do not eat me signal, is elevated in a variety of human cancers. On the other hand, the expression of CD163, a scavenger receptor, is increased in the M2-like TAM, and studies suggested that M2 macrophages phagocytose antibody opsonized target cancer cells more efficiently than M1 macrophages (27, 28). Despite wild speculation, systemic examination of macrophage function in pathogenesis of PDA has been scarce. In our current studies, using primary human pancreatic cancer as a model, we found that the phagocytosis function of PDA-TAMs is significantly impaired in comparison with macrophages isolated from control normal pancreatic tissue. We found that VentX expression is drastically reduced in TAMs of all tested cases of PDA. The significance of the study was suggested by the findings that restoration of VentX expression in PDA-TAMs revokes TAM phagocytosis function and that VentX-TAMs transform immunity by alternating the molecular and cellular composition at PDA-TME. Interestingly, mechanistic exploration showed that VentX expression did not altered the expression of SIRP, the cellular receptor of CD47. On the other hand, we did find that ectopic expression of VentX inhibits phosphorylation of SHP-1 and SHP-2, the SIRP downstream signaling molecules implicated in inhibition of phagocytosis. Moreover, our

data showed that VentX promote the expression of TLRs and downstream signaling molecules as well as FAK signaling, which has been implicated in promoting phagocytosis. Our data is consistent with the prior notion of the M1 and M2 signaling in regulating phagocytosis. We show here that this process is controlled by VentX, a human homologue of the *Xenopus* ventral homeobox protein Xom (29-31). Since the initial discovery of macrophages as the key regulator of immunity more than one hundred years ago, the cell intrinsic factor that control macrophage plasticity has remained elusive (32, 33). By leveraging the power of developmental study, which led to the discovery of the VentX as the key regulator of macrophage plasticity (14, 17, 18, 30, 31, 34), our current findings suggested a fundamental mechanism of immune regulation, which underlies the central mechanism of immune suppression at PDA-TME. Currently, the mechanism underlying decreased VentX expression in PDA-TAMs remained unknown. Our data suggested that further exploration along this line may provide better mechanistic insight and potential novel therapeutic opportunities to improve PDA prognosis.

Material and Methods

Collection of pancreatic tissue samples

A total of 19 patients with pancreatic adenocarcinoma, who were scheduled for surgical resection at Brigham and Women's Hospital, were consented to have a portion of resected tissues and blood collected for research purposes. All patients signed an informed consent document that was approved by the Institutional Review Board of Brigham and Women's Hospital. The characteristics of the pancreatic cancer patients whose specimens were used for this study were listed in Table 1. Around 5-10gram tissues were collected from tumor mass, or adjacent normal tissues. Tumor samples and control tissues were verified by board certified pathologists at the institution.

Preparation of lymphocytes and macrophages from pancreatic and tumor tissues

Lymphocytes were isolated essentially as described (14 Le, 2018 #1082, 35). Briefly, dissected fresh normal pancreatic tissues and pancreatic tumors were rinsed in 10-cm Petri dish with Ca^{2+}-free and Mg^{2+}-free hank's balanced salt solution (HBSS) (life technologies) containing 2% fetal bovine serum (FBS) and 2 mM Dithiothreitol (DTT) (Sigma-Aldrich). The pancreatic and tumor tissues were then cut into around 0.1 cm pieces by a razor blade and incubated in 5 mL HBSS containing 5 mM EDTA (Sigma-Aldrich) at 37ºC for 1 hour. The tissues were then passed through a gray-mesh (100 micron). The flow-throughs containing lymphocytes and epithelial cells were then analysis by a flow cytometer.

To isolate the macrophages, normal pancreatic tissues and pancreatic tumors were rinsed with HBSS, cut into around 0.1 cm pieces by a razor blade and then incubated in HBSS (with Ca^{2+} and Mg^{2+}), containing 2% FBS, 1.5 mg/mL Collagenase D (Roche), 0.1 mg/mL Dnase I at 37ºC for 1 hour. The digested tissues were then passed through a gray-mesh (70 micron) filter. The flow-throughs were collected, washed, and resuspended in RPMI 1640 medium. Normal tissue macrophages and TAMs were further purified using EasySep™ Human Monocyte/Macrophage Enrichment kit without CD16 depletion (StemCell Technologies, Cat# 19085**)** according to the manufacturer's instructions. The isolation process does not lead to activation of macrophages and the purity of isolated

macrophages was above 95% (14, 35, 36). More than 98% of cells isolated by the techniques were viable by propidium iodide (PI) staining tests.

FACS analysis

Phenotypic analysis of macrophages and lymphocytes was performed using flow cytometry after immunolabeling of cells with fluorescence dye–conjugated antibodies. The following antibodies were used: PE-conjugated anti-CD3 (OKT3), -CD25 (BC96), -CD14 (61D3), -CD40 (5C3), -CD80 (2D10.4), -CD163 (GH161), -PD-1L (J105), and FITC-conjugated anti-CD4 (RPA-T4), and -CD68 (Y182A), and APC-conjugated anti-CD8 (OKT8), -CD4 (OKT4) and -SIRPα (15-414) (eBioscience, Inc). Intracellular staining of anti-Foxp3 (236A/E7)-APC and -IFN-γ (4S.B3)-PE antibodies was performed following the protocol provided by manufacturer. Isotope control labeling was performed in parallel. Antibodies were diluted as recommended by the supplier. Labeled cells were acquired using the BD LSRFortessa at the Flow Cytometry Core of the Dana Farber Cancer Institute with the FACS Diva software (BD Biosciences) and analyzed using the FlowJo 10.1 software (Treestar). Typically, 20,000 cells were analyzed per sample according to the standard FACS analysis procedure. Results are expressed as the percentage of positive cells.

Quantitative RT-PCR

Total RNA was isolated by the TRIzol reagent (Life Technologies) and RNA amounts were measured by NanoDrop 2000 (Thermo Scientific). Equal amount of RNA was used for first-strand cDNA synthesis with SuperScript III First-Strand Synthesis System (Life Technologies) according to the manufacturer's protocol. The AccuPrime Taq DNA polymerase system (Life Technologies) was used to amplify VentX cDNA with conventional PCR. Quantitative measurements of VentX and other cDNA were carried out with SYBR Green, using a Mastercycler ep Gradient S (Eppendorf). GAPDH was used as a house keeping gene to normalize mRNA expression. The primers used were listed in supplemental table 1. Relative expression profiles of mRNAs were calculated using the comparative Ct method (DDCT method).

Cytokine measurement

Levels of IL-1β and TNF-α were quantified using ELISA kits obtained from eBiosciences. Analyses were conducted according to the manufacturer's instructions. Triplicate wells were plated for each condition. Nitrite concentrations in tissue culture supernatants were determined using Griess reagent kit (Molecular Probes), as described previously (14).

Transfection Assays

Plasmids encoding GFP-VentX and control GFP were described previously (31). Transfection of GFP-VentX and GFP into macrophages were carried out using the Human Macrophage Nucleofector Kit (Catalog #: VVPA-1008, Lonza, Walkersville, MD). Briefly, 2×10^6 cells were re-suspended into 100 µl nucleofector solution with 5 µg of plasmid DNA for 20 minutes on ice. Transfections were performed in Nculeofector 2b Device (Lonza). After transfection, cells were placed on ice immediately for 1 minute and then cultured in pre-warmed RPMI 1640 complete medium, containing 10% FBS and 1% antibiotic-antimycotic solution (Gibco, Cat# 15240062) for 48 hours before transfected cells were used for experiments.

For VentX knock-down experiments, pancreatic TAMs were transfected with Morpholino oligonucleotides (MO) (Gene Tools, LLC, Philomath, OR) using the Human Macrophage Nucleofector Kit (Lonza, Walkersville, MD) as previously described (14, 18). Briefly, 2×10^6 cells were re-suspended into 100 µl nucleofector solution with 2.5 nmol of either VentX MO: 5'-TACTCAACCCTGACATAGAGGGTAA-3' or a control MO oligonucleotide: 5'-CCTCTTACCTCAGTTACAATTTATA-3' and electroporated with the Nucleofector II Device (Lonza). Cells were then immediately removed from the device and placed on ice for 1 minute. The cells were then incubated overnight with 1ml pre-warmed Human Monocyte Nucleofector Medium containing 2mM glutamine and 10% FBS. Cells were then re-suspended into complete RPMI medium and stimulated with 10 ng/mL of LPS (Sigma-Aldrich) or control PBS overnight for phagocytosis assays.

Phagocytosis assays

For the phagocytosis assay, PANC-1 cells (human pancreatic cancer cell line, Sigma-Aldrich) or primary human leukemia cells (Brigham and women's Hospital) were

labeled with 1µM of CFSE Yellow using the CellTrance CFSE proliferation kit (Fisher Scientific). 5 x 10^5 TAMs transfected with GFP or GFP-Ventx were plated in each well of 12-well tissue culture plates (Coring). The TAMs were then incubated in RPMI complete medium for 2 hours before mixing with 1 x 10^6 of CSFE yellow labeled cancer cells. After indicated incubation time, the TAMs were washed repeatedly and detached by 0.25% Trypsin/EDTA and phagocytosis was analyzed by a flow cytometer. Microscopic analysis of phagocytosis was performed with a Nikon Eclipse Ti fluorescence microscopy. Images were captured at magnification of 20 × or 40 × using a color camera and the NIS Elements imaging software (Nikon). Brightness and contrast for representative images were adjusted equally among groups.

Western blot analysis

Western blot analysis was performed as described previously (14, 18). Briefly, total cells were lysed in 1× RIPA buffer (Abcam Inc) mixed with phosphatase and protease inhibitor cocktails (Cell Signaling Technology, CST). Proteins were resolved by 4-15% Tris-Glycine Gel (Bio-Rad) electrophoresis. Primary antibodies used included VentX (Abcam Inc, ab105352, 1:500), β-actin (CST, 4967, 1:2000), anti-phospho-SHP-1(Tyr564) (CST, Cat#8849, 1:500), SHP-2(Tyr542) (CST, Cat#3751, 1:500), phosphor-FAK(Tyr397) (CST, Cat#3283, 1:500) antibodies and their protein control antibodies; SHP-1(CST, Cat#3759, 1:1000), SHP-1 (CST, Cat#3397, 1:1000 and FAK CST, Cat#3285, 1:1000).

T cell proliferation assays

T- cell proliferation were performed essentially as described (18, 37). Briefly, blood CD8 cells of pancreatic patients were enriched by Easysep human CD8 enrichment kit following the manufacturer's instructions (StemCell Technologies, Cat#19053). 1 x 10^6 CD8 cells were labeled with 1µM of CFSE Yellow and then activated with human T-Activator CD3/CD28 Dynabeads (Gibco, Cat# 11131D) at a beads to T-cell ratio of 1:4 in the presence of 10 ng/ml IL-2 (PeproTech, Rocky Hill, NJ). Activated CD8 were then mixed with 0.25 x 10^6 GFP-VentX or GFP transfected TAMs of the same patients. The mixtures were incubated in completed RPMI 1640 at 37ºC, 5% CO_2 for 5 days. Cells were then stained with an anti-CD8-APC conjugated antibody and analyzed by a flow cytometer.

Co-cultures of tumor tissues and macrophages

Tumor tissue were washed with 1× PBS buffer plus antibiotics and then cut into 0.5 cm pieces. Tissues were mix cultured with 0.5 x 10^6 GFP-VentX or GFP transfected macrophages of the same patient in 2 mL of RPMI 1640 completed medium, supplemented with 1% antibiotic-antimycotic solution (Gibco). The cultures were incubated at 37ºC, 5% CO_2 for 5 days. The tissues were then subjected to cell isolation and analyzed by a flow cytometry, or immunohistochemistry studies.

NSG-PDX model of human pancreatic cancers

Animal models of primary human pancreatic cancers were developed as described previously (38). All animal experiments were approved by the Institutional Animal Care and Use Committee at the Brigham and Women's Hospital. Briefly, 8-week-old NOD.Cg-*Prkdc*^{scid} *Il2rg*^{tm1Wjl}/SzJ mice (commonly known as NOD scid gamma, or NSG mice) were purchased from the Jackson Laboratory and maintained under specific pathogen-free conditions. Pancreatic tumors were cut into around 0.5 cm pieces and then surgically implanted into subcutaneous space on the dorsal side of NSG mice. After one week of implantation, 0.5 × 10^6 TAMs transfected with GFP-VentX or control GFP were injected into the mice through tail vain. The tumor growth was monitored twice weekly and measured by a caliper for 6 weeks.

In vivo tracing of injected TAMs was carried out using CFSE stained TAMs or macrophages, according to the manufacture's instruction (Molecular Probes, Eugene, OR). Briefly, 1 × 10^6 TAMs were incubated in 5 mL of 5 μM CFSE staining solution in a 37°C water bath for 20 minutes. Cells were then incubated with 20 ml of RPMI 1640 completed medium for 5 minutes to removed unbounded dye. After centrifugation, cells were dissolved in PBS and then tail-vain injected into NSG mice. Tumor tissues and lymph nodes were dissected out 3 days after injection and TAMs were isolated as CFSE positive cells.

Immunohistochemistry

Immunohistochemistry were performed following established protocol (39). Briefly, pancreatic tumors or adjacent normal tissues were fixated in formalin (Fisher

Scientific Company, Kalamazoo, MI) for at least 48 hours. The tissues were then embedded in paraffin and sectioned. CD8 (Dako, Carpinteria, CA, clone C8/144B, 1:100), CD163 (Vector, clone 10D6, 1:250) and Vimentin (Dako, clone M0725, 1:50) and Haematoxylin/eosin (H&E) staining were performed at Specialized Histopathology Core at Dana-Farber/Harvard Cancer Center. All IHC was performed on the Leica Bond automated staining platform, using the Leica Biosystems Refine Detection Kit with EDTA antigen retrieval. The images of whole slides were scanned by Pannoramic MIDI II digital slide scanner and analyzed with Caseviewer and Quant center software (3DHistech).

Statistical Analysis

Student's test or one-way ANOVA were used for statistical analysis in Prism version 8 (GraphPad, La Jolla, CA). Data were presented as mean ± standard deviation (SD). Tumor growth curves were analyzed by repeated measurement two-way ANOVA using Sidak's multiple comparison test. The level of significance was indicated by the *p* value. In all figures, levels of statistical significance were indicated as: $*p < 0.05$, $**p<0.01$.

Study Approval

All patients signed an informed consent document that was approved by the Institutional Review Board of the Brigham and Women's Hospital, Boston, MA. Tumor samples and control tissues were verified by board certified pathologists at the institution. IRB study Number is 2006P1354. All animal experiments were approved by the Institutional Animal Care and Use Committee at the Brigham and Women's Hospital. Animal Approval Number is 2016N000353.

Author contributions

Y.L.,H.G.,Z.Z. designed the research, analyzed the data, prepared figures. Y.L.,H.G. performed the experiments. R.B.,B.R.L.Z.T.C. provided tumor samples and clinical information and analysis. Z.Z. wrote the manuscript.

Acknowledgments

We thank Marc Kirschner for critical discussion, Paul Yu for the use of equipment. We thank Dana-Farber/Harvard Cancer Center in Boston, MA, for the use of the Specialized Histopathology Core, which provided histology and immunohistochemistry service. Dana-Farber/Harvard Cancer Center is supported in part by an NCI Cancer Center Support Grant # NIH 5 P30 CA06516. Z. Zhu was supported by research funds from Brigham and Women's Hospital.

Conflict of Interest Statement

The authors have declared that no conflict of interest exists.

References:

1. Hidalgo, M. 2010. Pancreatic cancer. *N Engl J Med* 362:1605-1617.
2. Polireddy, K., and Chen, Q. 2016. Cancer of the Pancreas: Molecular Pathways and Current Advancement in Treatment. *J Cancer* 7:1497-1514.
3. Soares, K.C., Rucki, A.A., Wu, A.A., Olino, K., Xiao, Q., Chai, Y., Wamwea, A., Bigelow, E., Lutz, E., Liu, L., et al. 2015. PD-1/PD-L1 blockade together with vaccine therapy facilitates effector T-cell infiltration into pancreatic tumors. *J Immunother* 38:1-11.
4. Rawla, P., Sunkara, T., and Gaduputi, V. 2019. Epidemiology of Pancreatic Cancer: Global Trends, Etiology and Risk Factors. *World J Oncol* 10:10-27.
5. Siegel, R.L., Miller, K.D., and Jemal, A. 2015. Cancer statistics, 2015. *CA Cancer J Clin* 65:5-29.
6. Fukunaga, A., Miyamoto, M., Cho, Y., Murakami, S., Kawarada, Y., Oshikiri, T., Kato, K., Kurokawa, T., Suzuoki, M., Nakakubo, Y., et al. 2004. CD8+ tumor-infiltrating lymphocytes together with CD4+ tumor-infiltrating lymphocytes and dendritic cells improve the prognosis of patients with pancreatic adenocarcinoma. *Pancreas* 28:e26-31.
7. Sharma, P., Wagner, K., Wolchok, J.D., and Allison, J.P. 2012. Novel cancer immunotherapy agents with survival benefit: recent successes and next steps. *Nat Rev Cancer* 11:805-812.
8. Vonderheide, R.H., and Bayne, L.J. 2013. Inflammatory networks and immune surveillance of pancreatic carcinoma. *Curr Opin Immunol* 25:200-205.
9. Hiraoka, N., Onozato, K., Kosuge, T., and Hirohashi, S. 2006. Prevalence of FOXP3+ regulatory T cells increases during the progression of pancreatic ductal adenocarcinoma and its premalignant lesions. *Clin Cancer Res* 12:5423-5434.
10. Ene-Obong, A., Clear, A.J., Watt, J., Wang, J., Fatah, R., Riches, J.C., Marshall, J.F., Chin-Aleong, J., Chelala, C., Gribben, J.G., et al. 2013. Activated pancreatic stellate cells sequester CD8+ T cells to reduce their infiltration of the juxtatumoral compartment of pancreatic ductal adenocarcinoma. *Gastroenterology* 145:1121-1132.
11. Ino, Y., Yamazaki-Itoh, R., Shimada, K., Iwasaki, M., Kosuge, T., Kanai, Y., and Hiraoka, N. 2013. Immune cell infiltration as an indicator of the immune microenvironment of pancreatic cancer. *Br J Cancer* 108:914-923.
12. Hu, H., Hang, J.J., Han, T., Zhuo, M., Jiao, F., and Wang, L.W. 2016. The M2 phenotype of tumor-associated macrophages in the stroma confers a poor prognosis in pancreatic cancer. *Tumour Biol* 37:8657-8664.
13. Blando, J., Sharma, A., Higa, M.G., Zhao, H., Vence, L., Yadav, S.S., Kim, J., Sepulveda, A.M., Sharp, M., Maitra, A., et al. 2018. Comparison of immune infiltrates in melanoma and pancreatic cancer highlights VISTA as a potential target in pancreatic cancer. *Proc Natl Acad Sci U S A* 116:1692-1697.
14. Wu, X., Gao, H., Ke, W., Giese, R.W., and Zhu, Z. 2011. The homeobox transcription factor VentX controls human macrophage terminal differentiation and proinflammatory activation. *J Clin Invest* 121:2599-2613.
15. Zhu, Y., Herndon, J.M., Sojka, D.K., Kim, K.W., Knolhoff, B.L., Zuo, C., Cullinan, D.R., Luo, J., Bearden, A.R., Lavine, K.J., et al. 2017. Tissue-Resident

Macrophages in Pancreatic Ductal Adenocarcinoma Originate from Embryonic Hematopoiesis and Promote Tumor Progression. *Immunity* 47:597.
16. Mantovani, A., Marchesi, F., Malesci, A., Laghi, L., and Allavena, P. 2016. Tumour-associated macrophages as treatment targets in oncology. *Nat Rev Clin Oncol* 14:399-416.
17. Wu, X., Gao, H., Bleday, R., and Zhu, Z. 2014. Homeobox transcription factor VentX regulates differentiation and maturation of human dendritic cells. *J Biol Chem*.
18. Le, Y., Gao, H., Bleday, R., and Zhu, Z. 2018. The homeobox protein VentX reverts immune suppression in the tumor microenvironment. *Nat Commun* 9:2175.
19. Gordon, S. 2016. Phagocytosis: An Immunobiologic Process. *Immunity* 44:463-475.
20. Bian, Z., Shi, L., Guo, Y.L., Lv, Z., Tang, C., Niu, S., Tremblay, A., Venkataramani, M., Culpepper, C., Li, L., et al. 2016. Cd47-Sirpalpha interaction and IL-10 constrain inflammation-induced macrophage phagocytosis of healthy self-cells. *Proc Natl Acad Sci U S A* 113:E5434-5443.
21. Gordon, S.R., Maute, R.L., Dulken, B.W., Hutter, G., George, B.M., McCracken, M.N., Gupta, R., Tsai, J.M., Sinha, R., Corey, D., et al. 2017. PD-1 expression by tumour-associated macrophages inhibits phagocytosis and tumour immunity. *Nature* 545:495-499.
22. Willingham, S.B., Volkmer, J.P., Gentles, A.J., Sahoo, D., Dalerba, P., Mitra, S.S., Wang, J., Contreras-Trujillo, H., Martin, R., Cohen, J.D., et al. 2012. The CD47-signal regulatory protein alpha (SIRPa) interaction is a therapeutic target for human solid tumors. *Proc Natl Acad Sci U S A* 109:6662-6667.
23. Zhong, Y.F., and Holland, P.W. 2011. The dynamics of vertebrate homeobox gene evolution: gain and loss of genes in mouse and human lineages. *BMC Evol Biol* 11:169.
24. Mantovani, A., Bottazzi, B., Colotta, F., Sozzani, S., and Ruco, L. 1992. The origin and function of tumor-associated macrophages. *Immunol Today* 13:265-270.
25. Franklin, R.A., Liao, W., Sarkar, A., Kim, M.V., Bivona, M.R., Liu, K., Pamer, E.G., and Li, M.O. 2014. The cellular and molecular origin of tumor-associated macrophages. *Science* 344:921-925.
26. Feng, M., Jiang, W., Kim, B.Y.S., Zhang, C.C., Fu, Y.X., and Weissman, I.L. 2019. Phagocytosis checkpoints as new targets for cancer immunotherapy. *Nat Rev Cancer* 19:568-586.
27. Leidi, M., Gotti, E., Bologna, L., Miranda, E., Rimoldi, M., Sica, A., Roncalli, M., Palumbo, G.A., Introna, M., and Golay, J. 2009. M2 macrophages phagocytose rituximab-opsonized leukemic targets more efficiently than m1 cells in vitro. *J Immunol* 182:4415-4422.
28. Kneidl, J., Loffler, B., Erat, M.C., Kalinka, J., Peters, G., Roth, J., and Barczyk, K. 2012. Soluble CD163 promotes recognition, phagocytosis and killing of Staphylococcus aureus via binding of specific fibronectin peptides. *Cell Microbiol* 14:914-936.

29. Moretti, P.A., Davidson, A.J., Baker, E., Lilley, B., Zon, L.I., and D'Andrea, R.J. 2001. Molecular cloning of a human Vent-like homeobox gene. *Genomics* 76:21-29.
30. Gao, H., Wu, B., Giese, R., and Zhu, Z. 2007. Xom interacts with and stimulates transcriptional activity of LEF1/TCFs: implications for ventral cell fate determination during vertebrate embryogenesis. *Cell Res* 17:345-356.
31. Gao, H., Le, Y., Wu, X., Silberstein, L.E., Giese, R.W., and Zhu, Z. 2010. VentX, a novel lymphoid-enhancing factor/T-cell factor-associated transcription repressor, is a putative tumor suppressor. *Cancer Res* 70:202-211.
32. Mosser, D.M., and Edwards, J.P. 2008. Exploring the full spectrum of macrophage activation. *Nat Rev Immunol* 8:958-969.
33. Bronte, V., and Murray, P.J. 2015. Understanding local macrophage phenotypes in disease: modulating macrophage function to treat cancer. *Nat Med* 21:117-119.
34. Gao, H., Wu, X., Sun, Y., Zhou, S., Silberstein, L.E., and Zhu, Z. 2012. Suppression of Homeobox Transcription Factor VentX Promotes Expansion of Human Hematopoietic Stem/Multipotent Progenitor Cells. *J Biol Chem* 287:29979-29987.
35. Kamada, N., Hisamatsu, T., Okamoto, S., Chinen, H., Kobayashi, T., Sato, T., Sakuraba, A., Kitazume, M.T., Sugita, A., Koganei, K., et al. 2008. Unique CD14 intestinal macrophages contribute to the pathogenesis of Crohn disease via IL-23/IFN-gamma axis. *J Clin Invest* 118:2269-2280.
36. Rogler, G., Hausmann, M., Vogl, D., Aschenbrenner, E., Andus, T., Falk, W., Andreesen, R., Scholmerich, J., and Gross, V. 1998. Isolation and phenotypic characterization of colonic macrophages. *Clin Exp Immunol* 112:205-215.
37. Eruslanov, E.B., Bhojnagarwala, P.S., Quatromoni, J.G., Stephen, T.L., Ranganathan, A., Deshpande, C., Akimova, T., Vachani, A., Litzky, L., Hancock, W.W., et al. 2014. Tumor-associated neutrophils stimulate T cell responses in early-stage human lung cancer. *J Clin Invest* 124:5466-5480.
38. Mittal, V.K., Bhullar, J.S., and Jayant, K. 2015. Animal models of human colorectal cancer: Current status, uses and limitations. *World J Gastroenterol* 21:11854-11861.
39. Wong, H.H., and Chu, P. 2012. Immunohistochemical features of the gastrointestinal tract tumors. *J Gastrointest Oncol* 3:262-284.

Figure 1

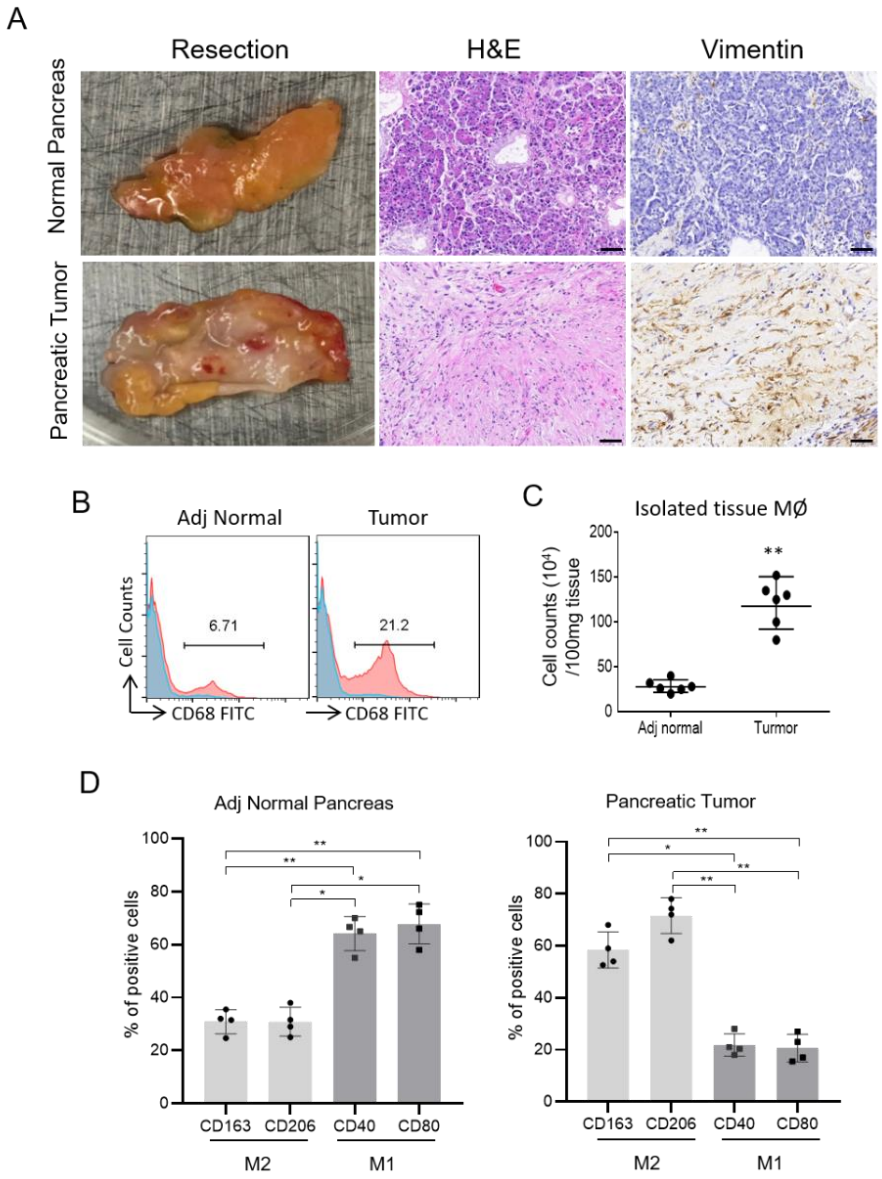

Figure 1. Characterization of pancreatic ductal adenocarcinoma (PDA). (A) Representative images of a pancreatic ductal adenocarcinoma (PDA) and a control adjacent normal pancreatic tissue. H&E and Vimentin immuno-staining of PDA and adjacent normal pancreatic tissue. Scale bar: 200 µm. **(B)** FACS analysis of CD68+ macrophages in pancreatic cancers. CD68+ macrophages in adjacent normal pancreatic tissue and PDA were analyzed by a flow cytometer. Blue shaded peaks were isotype control, red shaded peaks were CD68+ cells. **(C)** Accounting of CD68+ macrophages in pancreatic cancer and adjacent normal pancreatic tissues. n=6. Statistical significance was defined as ** p<0.01, calculated by paired Student's t test. **(D)** The percentage of surface expression of M2 markers (CD163 and CD206) and M1 surface markers (CD40 and CD80) on CD68+ macrophages of adjacent normal pancreatic tissues and TAMs from PDA of the same patients. Data shown are the means ± SD of 4 independent experiments, and one-way ANOVA with multiple comparisons was performed. * p < 0.05,** p<0.01.

Figure 2

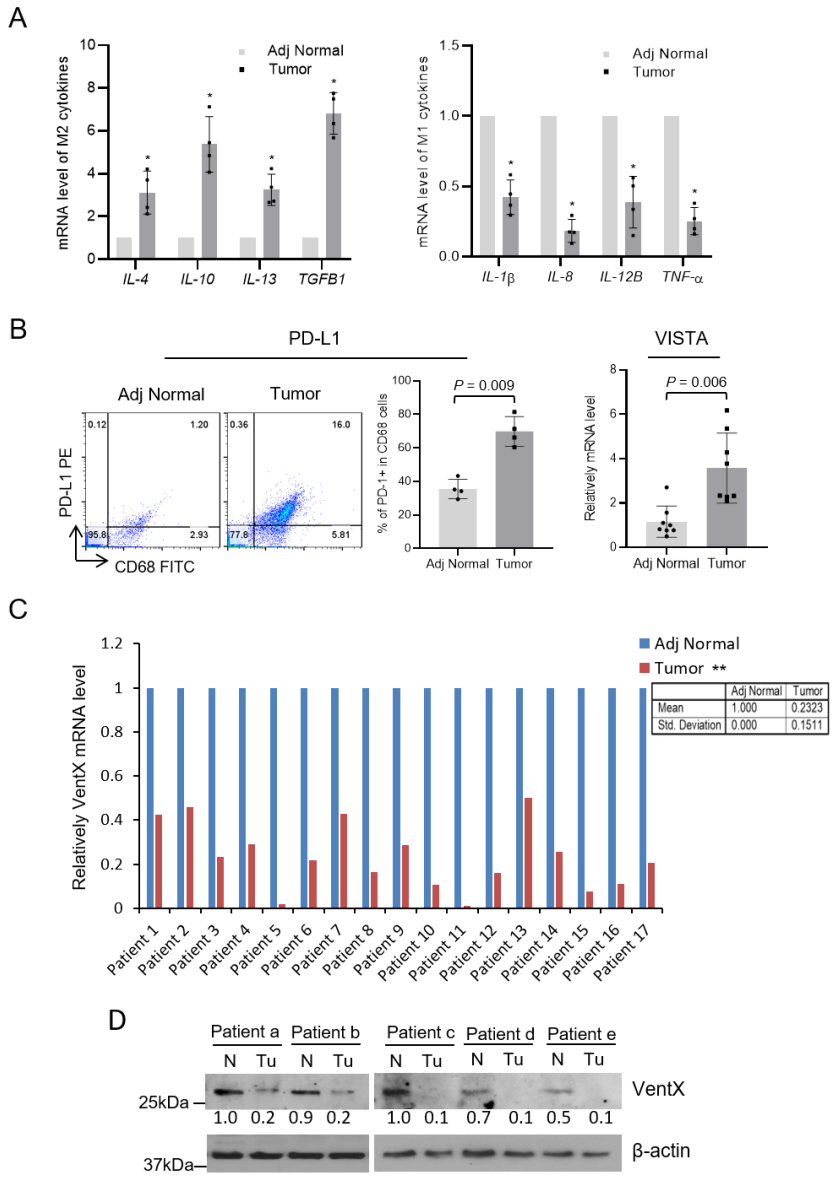

Figure 2. Characterization of tumor associated macrophages (TAMs) in pancreatic ductal adenocarcinoma (PDA). (A) The mRNA expression levels of indicated M1- and M2- cytokines in TAMs vs control macrophages as determined by qRT-PCR. Results represent mean ± SD of four independent experiments. * indicates $p < 0.05$ by paired Student's *t* test. **(B)** Cell surface expression of checkpoint inhibitor PD-L1 and mRNA of Vista in TAMs and control macrophages isolated from adjacent normal pancreatic tissues. The expression level of PD-L1 was determined by flow cytometer analysis, representative Figure was shown, n=4. The mRNA expression levels of Vista were determined by qRT-PCR. Results represent mean ± SD of eight independent experiments. ** indicates $p < 0.01$ by paired Student's *t* test. **(C)** Paired comparison of qRT-PCR measurement of VentX mRNA expression in macrophages isolated from normal control tissues and TAMs of 17 patients. The relative VentX mRNA expression levels in normal macrophages were arbitrarily designated as 1. ** indicates $p < 0.01$ TAMs vs. adjacent normal macrophages, n = 17 by paired Student's *t* test. **(D)** Western blot analysis of endogenous VentX protein levels in macrophages isolated from normal control tissues and TAMs of 3 patients. The numbers indicate the relative fold difference of VentX proteins as determined by *Image-J* software scanning.

Figure 3

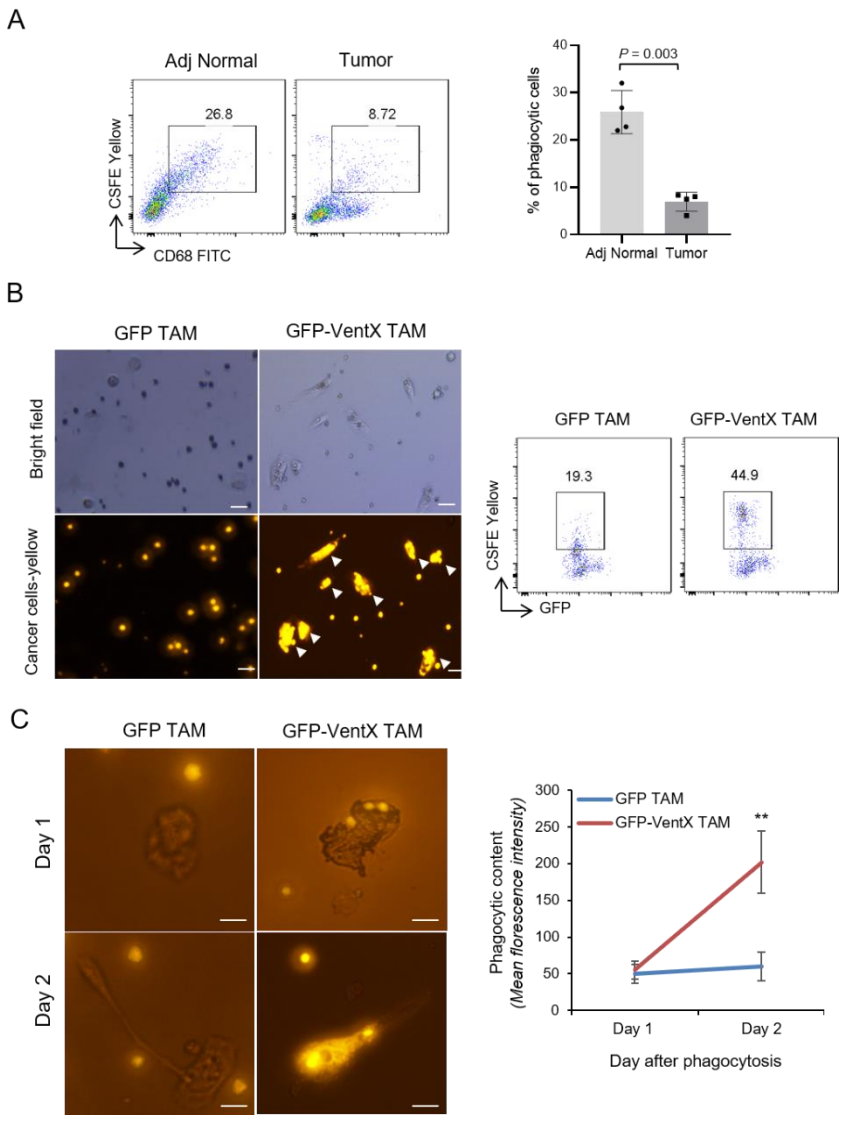

Figure 3. VentX promotes TAM phagocytosis. (A) Quantification of phagocytosis activity of TAM and control macrophage. Freshly isolated TAMs and control macrophages were incubated with 1 μM CFSE-Yellow labeled Panc-1 cells. The rate of phagocytosis was determined by flow cytometry. Data shown are the mean ± SD from 4 independent experiments. $p < 0.01$, by paired Student's *t* test. **(B)** VentX promotes TAM phagocytosis. TAMs were isolated and transfected with plasmids encoding GFP or GFP-VentX. The transfected TAMs were then incubated with 1 μM CFSE-Yellow labelled cancer cells for 24 hours. The effects of the treatment were determined by phase contrast and fluorescent microscopy (left) and flow cytometry analysis (right). Arrows indicated phagocytosed cancer cells. Scale Bar: 50μM. The representative figure was shown, n=3. **(C)** Phagocytosis and intracellular digestion of CFSE-Yellow labeled Panc-1 cells. TAMs transfected with control GFP or GFP-VentX were incubated with CFSE-Yellow labeled Panc-1 cells. Representative images of the phagocytosis were revealed by fluorescent microscopy after 24 hours (upper panel) and 48 hours (lower panel). Scale Bar: 20μm. Quantification of phagocytotic cells was performed by measuring green fluorescence intensity after phagocytosis. The graph represents the pixel intensity of fluorescence. Data presented are means ± SD, n=3, At least 10 cells were scanned for each time point.

Figure 4

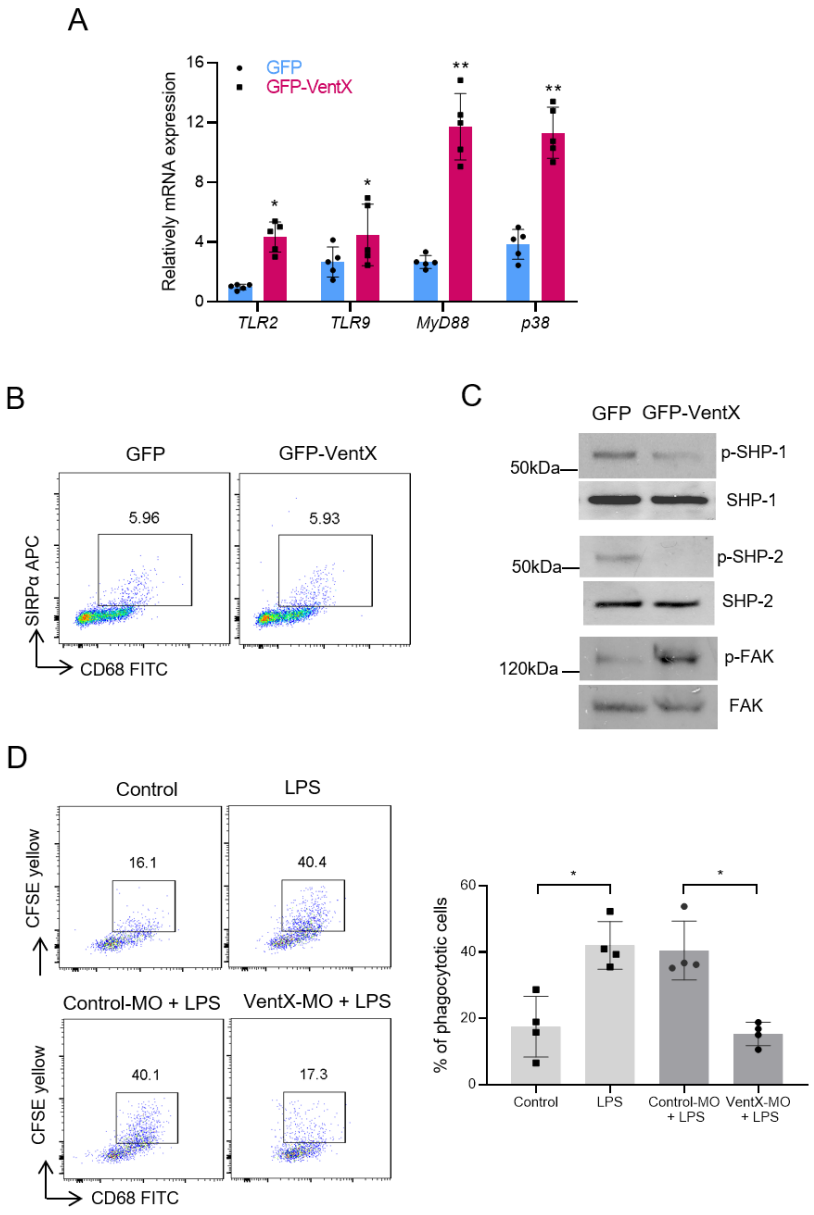

Figure 4. Effects of VentX on the expression of cell surface receptors and signaling molecules implicated in phagocytosis. (A) Effects of VentX on the expression of Toll like receptors and signaling molecules. Pancreatic TAMs were transfected with plasmids encoding GFP control and GFP-VentX. The expression of indicated TLRs and signaling molecules were determined by qRT-PCR. Data shown are mean ± SD of 5 different experiments. Paired Student's *t* test was performed. ** indicates $p < 0.01$, *$p <$ 0.05. **(B)** FACS analysis of SIRPα receptor expression on TAMs transfected with plasmids encoding GFP or GFP-VentX. **(C)** Western blot analysis of phosphorylation state as well as total protein of the intracellular signaling molecules SHP-1, SHP-2, FAK in GFP and GFP-VentX transfected TAMs. **(D)** Requirement of VentX for LPS stimulation of TAM phagocytosis. TAMs were isolated and transfected with morpholino oligo against VentX or control morpholino (MO) and then subjected to LPS stimulation. The effects of the treatment on phagocytosis were determined by flow cytometry.

Figure 5

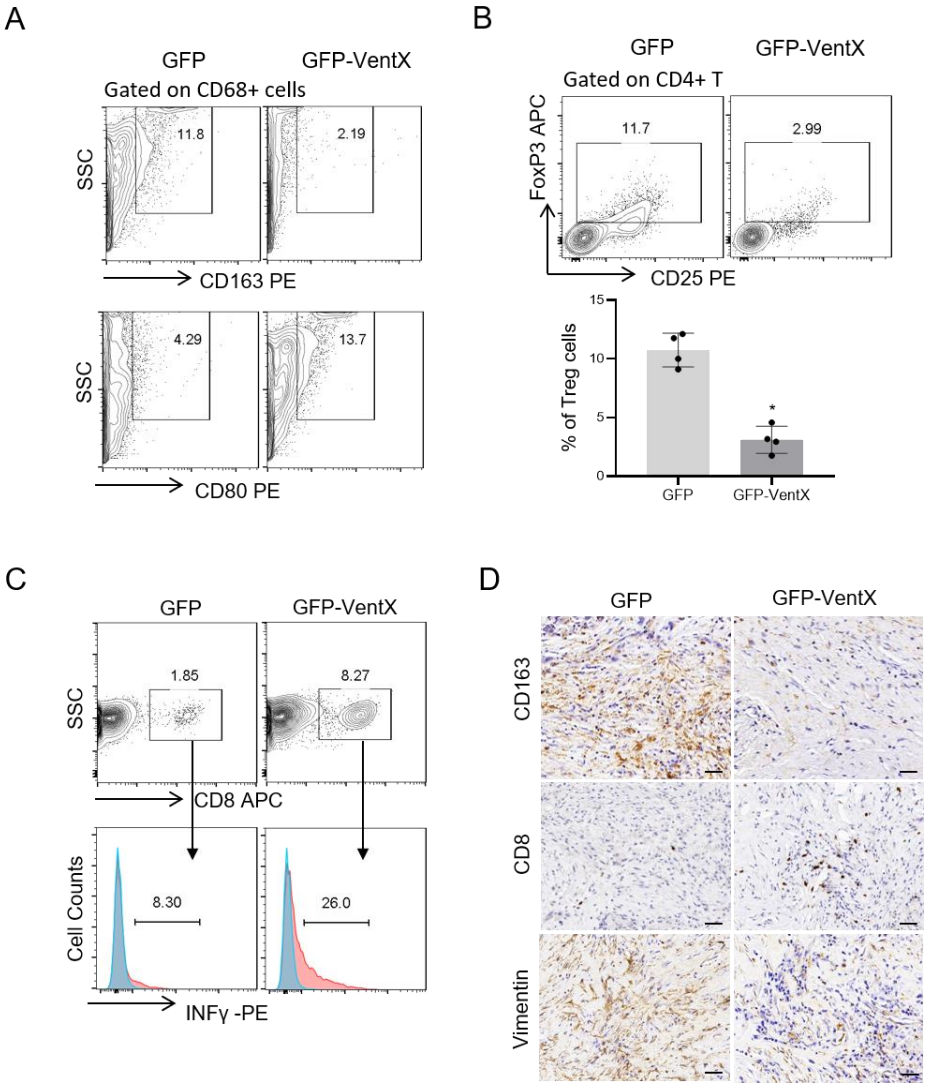

Figure 5. Effects of VentX-TAMs on PDA infiltrating immune cells at TME. (A) VentX-TAMs promotes M2 to M1 transition of PDA-TAMs. en block PDA tumor tissues were incubated with autologous TAMs transfected with GFP-VentX or GFP control. After 5 days incubation, the tumor endogenous TAMs were isolated and the percentage of M1-and M2- like TAMs were determined by FACS analysis of respective cell surface markers, CD80 and CD163 respectively; **(B)**, the effect of the incubation on Treg cell differentiation was determined by FACS analysis of percentage of CD4+CD25+Foxp3+ cells. Data represent the mean ± SD from 4 independent experiments. *$p < 0.05$, by paired Student's *t* test; **(C)** the effect of the incubation on proliferation (upper panel) and activation (lower panel) of CD8+ TIL cells were determined by FACS analysis of CD8 marker and IFN-γ expression respectively. **(D)** Effects of VentX-TAMs incubation on differentiation of PDA and infiltrating immune cells as revealed by immunohistochemical staining. Representative images were shown. Anti CD163, CD8 and Vimentin antibodies were used for the immune staining as indicated. Scale Bar: 100μm.

Figure 6

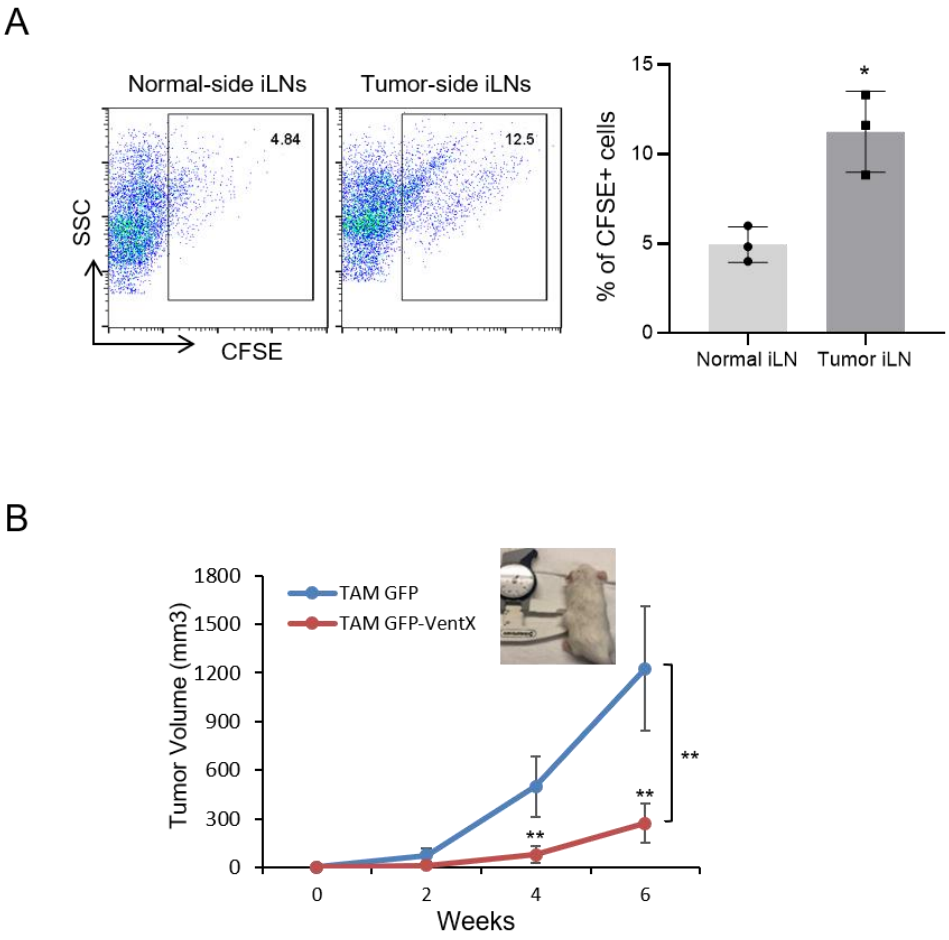

Figure 6. VentX-TAMs inhibits tumorigenesis of PDA in NSG-PDX models of primary human pancreatic cancers. NSG-PDX models of primary human pancreatic cancers were generated by subcutaneous implantation of small pieces of primary human PDA on the dorsal side of NSG mice. The mice were then tail-vein injected with VentX-TAMs or control GPF-TAMs. **(A)** Distribution of VentX-TAMs in lymph nodes. The CFSE-labeled VentX transfected TAMs were tail-vein injected into NSG-PDX mice of human PDA. 72 hours post-injection, inguinal lymph nodes (iLN) from tumor side or control side were removed from the mice and single cell suspensions were analyzed by flow cytometry. The percentage of CFSE-positive TAMs were shown. Data shown are mean ± SD of 3 independent experiments. Paired Student's *t* test was performed, $*p < 0.05$. **(B)** The growth of the PDA in vivo was observed up to 6 weeks and the results of the treatment were shown. Data represented mean of seven independent experiments (n=7), Statistics for mouse experiments were performed using Two-way ANOVA with repeated measures, $**p < 0.01$.

Table 1. Characteristics of pancreatic cancer patients, whose specimens was used in the study

Characteristics	Number (*n*=19)	(%)
Age, *y*		
≤ 60	2	10.5
60-79	15	79.0
≥ 80	2	10.5
Sex		
Male	12	63.2
Female	7	36.8
Pathology type		
Adenocarcinoma	19	100
Stage		
I	4	21.1
II	12	63.2
III	3	15.7
IV	0	0

Supplemental Figures and legends

Supplemental Figure 1

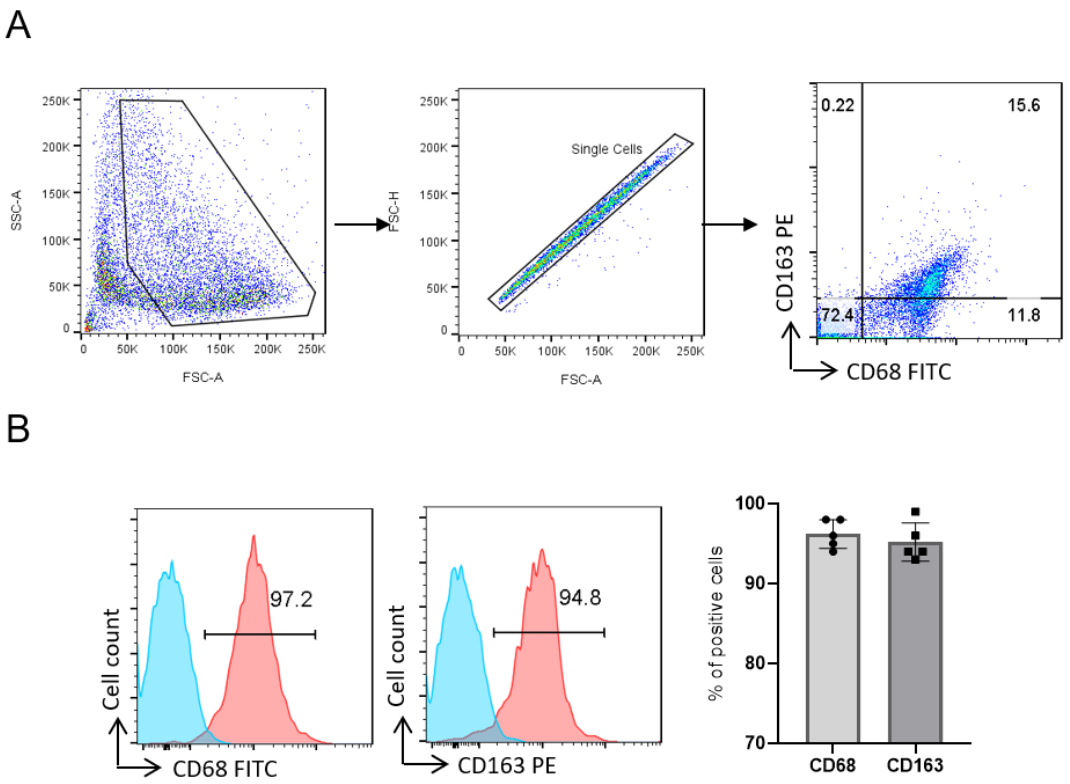

Supplemental Figure 1. Gating strategy and characterization of PDA-TAMs. (A) Gating strategy of FACS analysis. Mononuclear cells were gated on the basis of FCS-A versus SSC-A and then were sequentially gated to select single cells by FSC-A versus FSC-H. Subsequently, flow cytometry plots for the various markers were shown in biexponential format. **(B)** Purity of isolated TAMs. Mononuclear cells from tumor were used for TAM isolation process according to Material and Methods and purity of TAMs was determined by FACS analysis on indicated microphage markers. Data shown are means ± SD of 5 independent experiments

Supplemental Figure 2

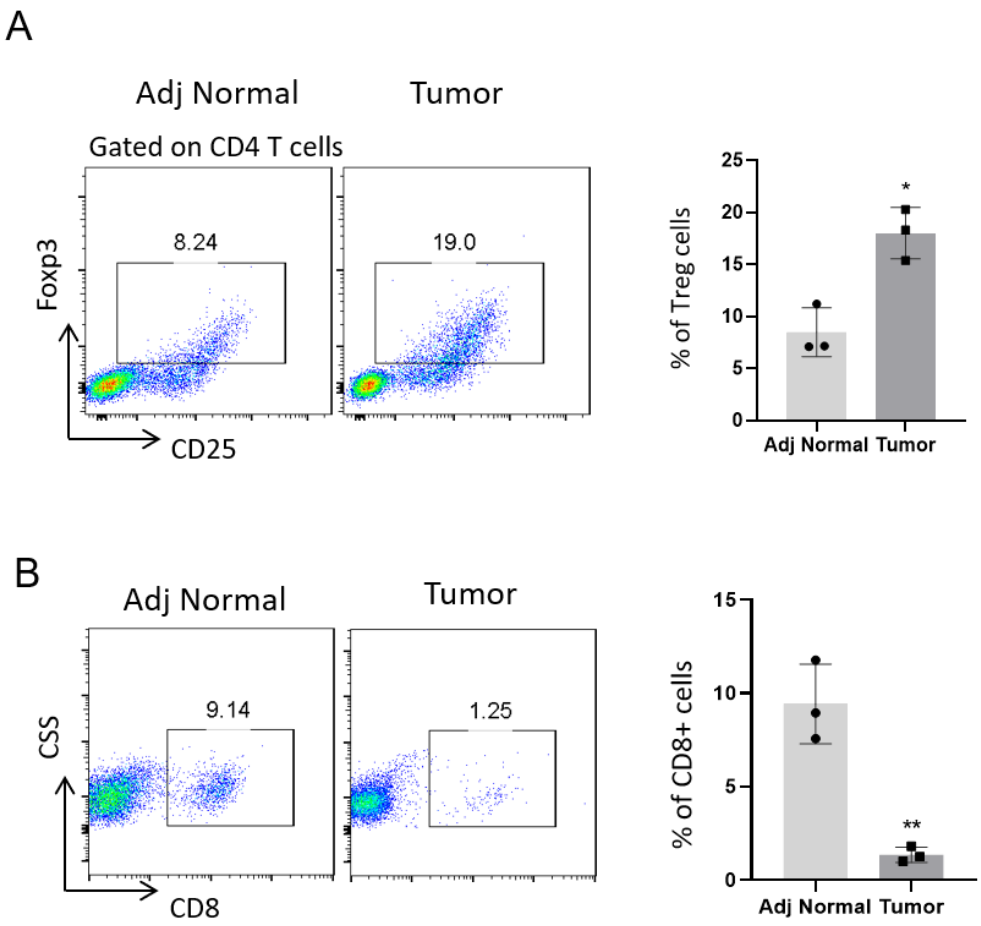

Supplemental Figure 2. Characterization of Treg and CD8 cells isolated from pancreatic tumors and adjacent normal pancreatic tissues. (A) Percentage of Treg cells in PDA and adjacent normal pancreatic tissues. Isolated tissue mononuclear cells were stained with anti-CD4-FITC, CD25-PE, Foxp3-APC and subjected to FACS analysis. The percentage of Treg (CD4+, CD25+, Foxp3+) cells was shown. **(B)** Percentage of CD8 cells in PDA and adjacent normal pancreatic tissues. Cells were stained with anti-CD8-PE and then subjected to FACS analysis. Data shown are means ± S.D. of three independent experiments, and paired Student's *t* test was performed. * P <0.05, ** P <0.01.

Supplemental Figure 3

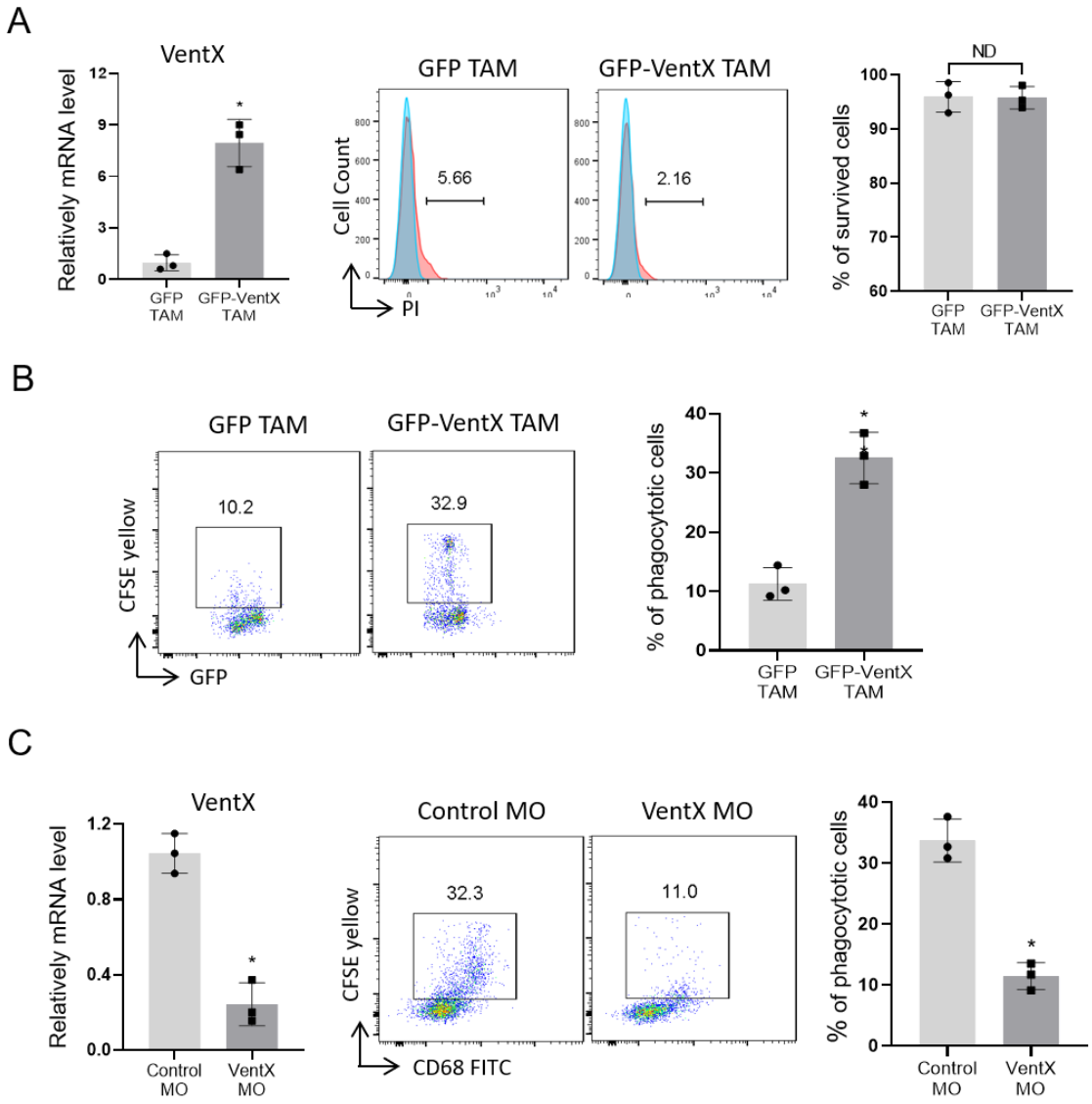

Supplemental Figure 3. VentX is required in TAMs for phagocytosis of leukemia cells.
(A) TAMs were transfected with GFP-VentX or GFP control. The VentX expression was determined by real-time PCR and cell viability was determined by PI staining. **(B)** TAMs were transfected with GFP-VentX or GFP control, and then incubated with CFSE-Yellow labelled leukemia cells at 1:2 ratio for 24 hours. Flow cytometric analysis were performed. Data represent the means ± SD from 3 independent experiments. *$p < 0.05$, by Student's *t* test. **(C)** Normal tissue macrophages were transfected with VentX-morpholino or morpholino control. The efficacy of VentX knock down was determined by qRT-PCR. The ratio of phagocytosis was determined by flow cytometry. Data shown are the means ± SD from 3 independent experiments. *$p < 0.05$, by paired Student's *t* test.

Supplemental Figure 4

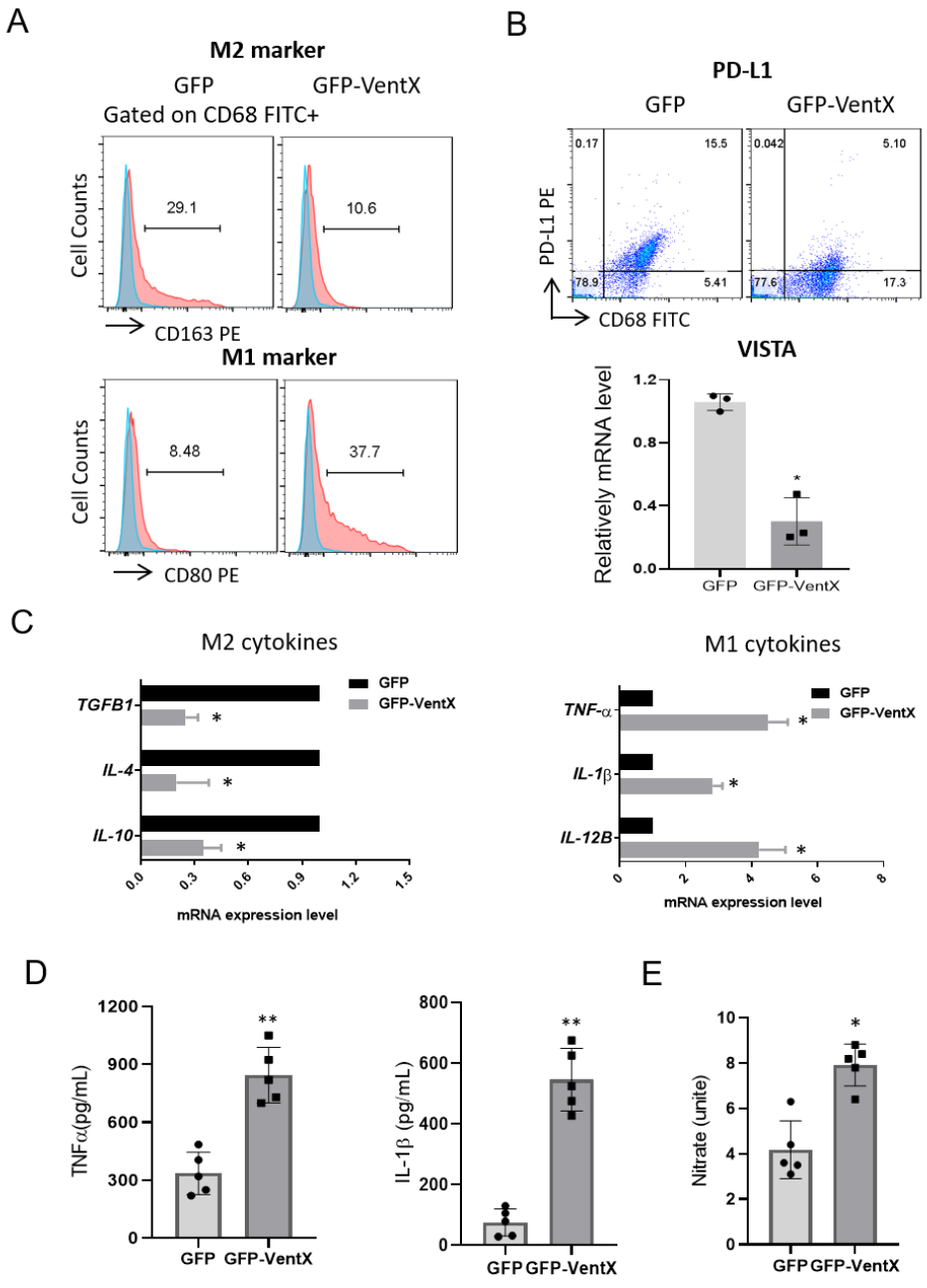

Supplemental Figure 4. Effects of VentX expression on TAM phenotype. Pancreatic TAMs were isolated and transfected with plasmids encoding GFP or GFP-VentX as described in material and methods. **(A)** The effects of VentX on the expression of M2 marker CD163 and M1 marker CD80 were determined by flow cytometry analysis. **(B)** The effects of VentX on the expression of PD-L1 and Vista was determined by FACS analysis and qRT-PCR respectively. **(C)** The effects of VentX on the expression of M2 and M1 cytokines as determined by qRT-PCR. Data represent means ± S.D. of three independent experiments, * $p < 0.05$. **(D)** TNF-α and IL-1β cytokine level and **(E)** Nitrate level from GFP-VentX or control GFP transfected TAMs. Results represent means ± S.D. of five independent experiments and paired Student's *t* test was used. * $p < 0.05$, ** $P < 0.01$ by Student *t* test.

Supplemental Figure 5

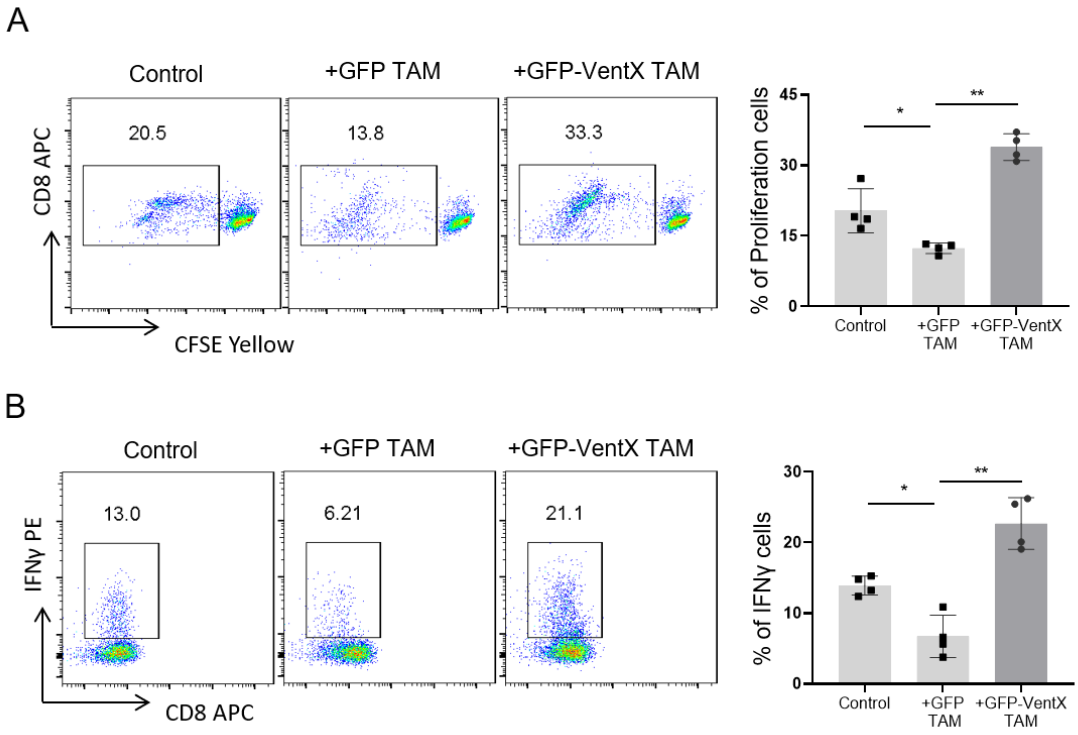

Supplemental Figure 5. VentX modulates TAM inhibition of CD8 TILs proliferation and activation. **(A)** Effects of VentX-modulated-TAMs on CD8 T cell proliferation. CFSE Yellow labelled CD8+ TIL T cells from PDA patients were stimulated with Dynabeads plus IL-2 and then cultured either alone or with autologous TAMs transfected with GFP or GFP-VentX at a T cells: TAMs ratio = 2:1 for 5 days. Representative results from 5 experiments were shown. The numbers on histograms represent the percentage of proliferating T cells; **(B)** the effects of VentX-modulated-TAMs on CD8 T cell activation was measured by FACS analysis of intracellular IFNγ. Data represent the means ± SD from 4 independent experiments. *$p < 0.05$, ** $p < 0.01$ by Student's *t* test.

Supplemental Figure 6

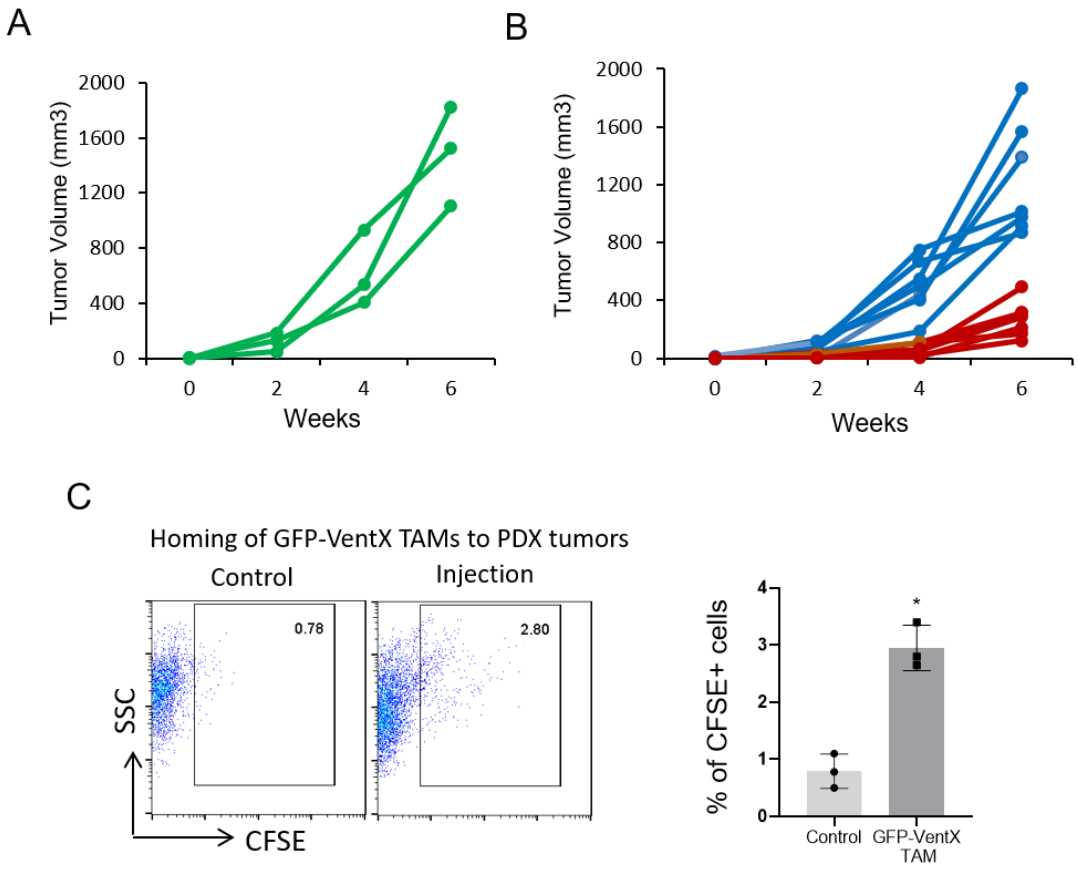

Supplemental Figure 6. Characterization of VentX-TAMs on tumorigenesis of PDA in NSG-PDX model of primary human pancreatic cancers. (A) Growth curve of individual primary human PDA in NSG-PDX mice. NSG-PDX models of primary human pancreatic cancers were generated by subcutaneous implantation of small pieces of primary human PDA on the dorsal side of NSG mice. The growth of the PDA in vivo was observed up to 6 weeks and the results of the PDA growth in each individual mice were shown, n=3 mice. **(B)** The NSG-PDX mice of primary human PDA were tail-vein injected with 0.5 million VentX-TAMs or control GPF-TAMs. The growth of PDA in each treated mice were shown individually. Red color lines indicated mice treated with VentX-TAMs. Blue color lines represented mice treated with control GFP-TAMs, n = 7 mice/group. **(C)** Accumulation of VentX-TAMs in PDA. The CSFE-labeled VentX transfected TAMs were tail-vein injected into NSG-PDX mice of human PDA. 72 hours post-injection, the PDAs were dissected out. The mononuclear cells were collected, and the presence of VentX-TAMs was revealed by CSFE positive cells. Data shown are means ± SD of 3 independent experiments, and paired Student's *t* test was performed. *$p < 0.05$.

Supplementary Table 1

Primer sequences used in this study

Gene name	Forward	Reverse
VentX-C*	AAGGCAATTAGGCGCTGCTT	ACAGAACAACTGAGTCCTCCA
VentX-R*	CCGTCAGCATCAAGGAGG	CTGGACCTCTGAGAGCTGC
IL1β	AAGCTGATGGCCCTAAACAG	AGGTGCATCGTGCACATAAG
GAPDH	AGAACGGGAAGCTTGTCATC	GCCTTCTCCATGGTGGTG
IL8	ATGACTTCCAAGCTGGCCGT	CCTCTTCAAAAACTTCTCCACA
IL12B	GCAGAGGCTCTTCTGACCCCCA	AGCTGACCTCCACCTGCCGA
TNFα	CGC CAC CAC GCT CTT CTG	GCC ATT GGC CAG GAG GGC
IL4	GCTTCCCCCTCTGTTCTTCC	CTGCTCTGTGAGGCTGTTCA
IL10	GATCCAGTTTTACCTGGAGGAG	CCTGAGGGTCTTCAGGTTCTC
IL13	CCTCTACAGCCCTCAGGGAG	ATCTTGGGAATCACCCACCC
TGFB1	TACCTGAACCCGTGTTGCTCTC	GTTGCTGAGGTATCGCCAGGAA
Vista	CCACCATGGCAACTTCTCCA	GAGTGGTGGTGCCTGATCTC
TLR2	TCTCCCATTTCCGTCTTTTT	GGTCTTGGTGTTCATTATCTTC
TLR9	CGCCAACGCCCTCAAGACA	GGCGCTTACATCTAGTATTTGC
MyD88	GAATCTTCCAAAGCGCAAAG	AGGATGACAAACTCCAAGCA
MAPKp38	AAGACTCGTTGGAACCCCAG	TCCAGTAGGTCGACAGCCAG
	C*: conventional PCR; R*: real-time PCR	